ACS Medicinal Chemistry Letters

pubs.acs.org/acsmedchemlett

Letter

Conformational-Design-Driven Discovery of EZM0414: A Selective, Potent SETD2 Inhibitor for Clinical Studies

Published as part of the ACS Medicinal Chemistry Letters special issue "Epigenetics 2022".

Joshua S. Alford, John W. Lampe, Dorothy Brach, Richard Chesworth, Kat Cosmopoulos, Kenneth W. Duncan, Sean T. Eckley, Jeffrey L. Kutok, Alejandra Raimondi, Thomas V. Riera, Brian Shook, Cuyue Tang, Jennifer Totman, and Neil A. Farrow*

Cite This: *ACS Med. Chem. Lett.* 2022, 13, 1137−1143

Read Online

ACCESS | Metrics & More | Article Recommendations | Supporting Information

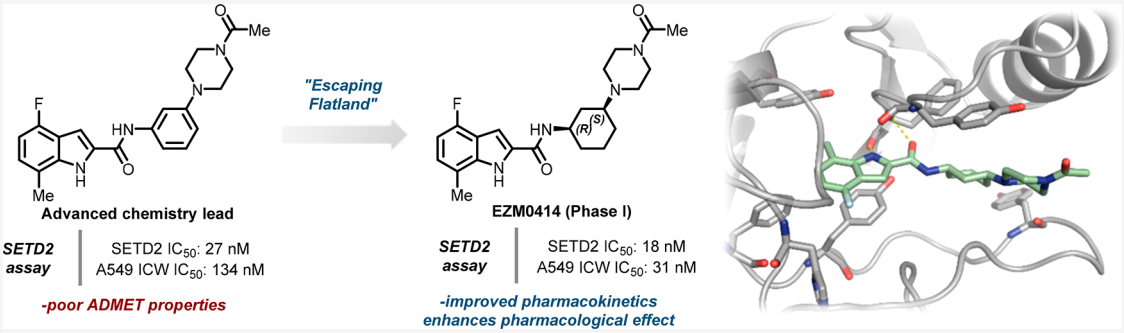

ABSTRACT: SETD2, a lysine *N*-methyltransferase, is a histone methyltransferase that plays an important role in various cellular processes and was identified as a target of interest in multiple myeloma that features a t(4,14) translocation. We recently reported the discovery of a novel small-molecule SETD2 inhibitor tool compound that is suitable for preclinical studies. Herein we describe the conformational-design-driven evolution of the advanced chemistry lead, which resulted in compounds appropriate for clinical evaluation. Further optimization of this chemical series led to the discovery of EZM0414, which is a potent, selective, and orally bioavailable inhibitor of SETD2 with good pharmacokinetic properties and robust pharmacodynamic activity in a mouse xenograft model.

KEYWORDS: *Histone methyltransferase, SETD2*

Lysine *N*-methyltransferases (KMTs) are a unique class of enzymes that mediate the methylation of lysine residues of histones.[1] Within this class, KMTs can be further divided into two subsets: SET-domain-containing and non-SET-domain. SETD2 is a member of the former subset and is the only known histone methyltransferase (HMT) that can catalyze the deposition of the third methyl group onto the dimethylated state of lysine 36 of histone H3 (H3K36me2). This methylation results in the trimethylated state of lysine 36 of histone H3 (H3K36me3). While H3K36me3 is generally associated with active transcription, SETD2 also plays a role in various other cellular processes, including transcriptional elongation and regulation, alternative RNA splicing, DNA damage repair, and crosstalk with other histone modifications.[2] In addition, SETD2 has been shown to behave as a tumor suppressor, since homozygous loss-of-function mutations have been associated with tumorigenesis and/or chemoresistance in certain solid tumors, most notably in renal cell carcinoma.[2] While SETD2 may function as a classical tumor suppressor in the context of certain solid tumors, this is not true for SETD2's role in the development of hematological malignancies such as leukemia and lymphoma. In these disease settings, SETD2 loss-of-function mutations are consistently heterozygous, suggesting that a haploinsufficient tumor suppressor role for SETD2 and therapeutic potential of SETD2 inhibition may also exist.[3−9]

We proposed that inhibition of SETD2 could be exploited in B-cell malignancies where perturbation of lysine 36 of histone H3 (H3K36) methylation plays a key role, including histone H1 mutations in DLBCL, and in the setting of t(4;14) chromosomal translocations present in high-risk multiple myeloma.[10,11] In t(4;14) multiple myeloma, MMSET (also known as NSD2) is highly expressed as a result of the translocation and has been

Received: April 8, 2022
Accepted: May 31, 2022
Published: June 7, 2022

https://doi.org/10.1021/acsmedchemlett.2c00167
ACS Med. Chem. Lett. 2022, 13, 1137−1143

shown to play a critical role in tumorigenesis. MMSET is a histone methyltransferase that catalyzes H3K36me1 and H3K36me2 formation, causing increased levels of H3K36me2, the substrate for SETD2.[12,13] We hypothesized that inhibiting SETD2 would impair tumor growth in the setting of a t(4,14) translocation, which would establish the proof of concept in this and other B cell malignancies (*e.g.*, DLBCL) that may demonstrate dysregulated H3K36me3 or a dependence on SETD2.

In our recent report on the discovery of the SETD2 inhibitor tool compound EPZ-719, we focused primarily on exploration of the structure−activity relationship (SAR) with respect to the indole motif and the central core of the molecule, leading to SETD2 inhibitor **2** and the closely related analogues **3** and **3-F** (see Figure 1).[14] The unique binding mode of these aniline-

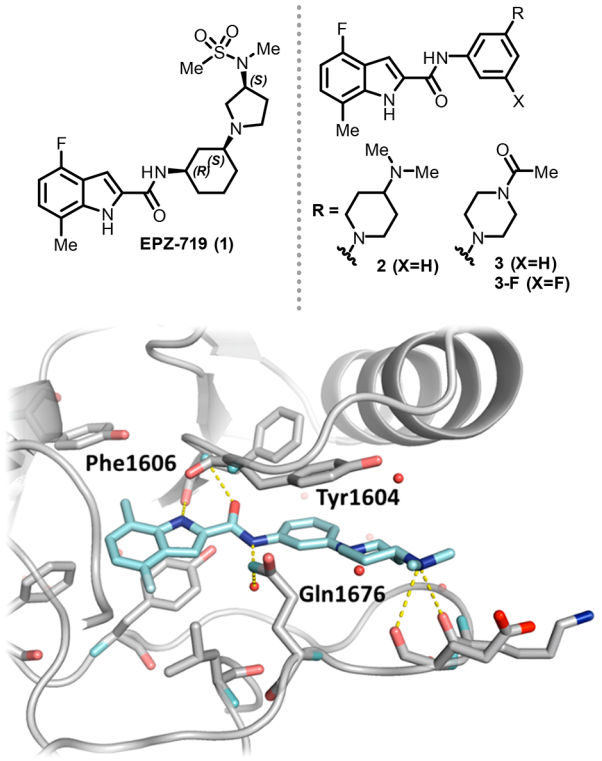

Figure 1. (top) Structures of SETD2 inhibitors **1**−**3**. (bottom) X-ray cocrystal structure of SETD2 and compound **2** (in pale cyan) (PDB ID 7LZD). Hydrogen bonds are shown with dotted yellow lines.

containing inhibitors was also disclosed in that report. Anilines are prevalent in modern drug discovery screening libraries because of their ease of synthesis, but this structural motif tends to impart less-than-ideal pharmacokinetic properties and potential metabolism-derived toxicities.[15] We reported that saturation of this ring significantly improved the physiochemical properties of the series and avoided the potential Ames toxicity; however, we did not detail the conformational studies leading us to the (1*R*,3*S*) stereochemistry seen in EPZ-719. The promising *in vivo* results with this tool compound led us to continue our work with this prototype in the pursuit of a suitable clinical candidate.[16]

The importance of reducing the basicity of the piperazine nitrogen with an electron-withdrawing group became apparent in our previous efforts to optimize the potency, selectivity, and PK properties of this early series.[14] Indolylcarboxamides **2** and **3** had been identified as promising leads with potent *in vitro* activity; however, translating that to *in vivo* potency proved to be challenging. In our cellular assay, indolylcarboxamide **3-F** (SETD2 biochemical IC_{50} = 12 nM and H3K36me3 ICW IC_{50} = 41 nM), a close analogue of **3**, was 6-fold more potent than **2** (SETD2 biochemical IC_{50} = 18 nM and H3K36me3 ICW IC_{50} = 235 nM), which lacked the electron-withdrawing group. While this optimization strategy continued to improve the cellular potency of analogues like **3**, the analogues continued to suffer from suboptimal PK profiles, with moderate to high clearance in mouse. We suspected that this was due to the high lipophilicity of the series. An overall increase in saturation is measured by F_{sp^3}, and the number of chiral centers in a molecule can improve its chance for clinical success.[17] This is likely due to a decrease in lipophilicity (highly lipophilic compounds (cLogP > 3; tPSA < 75) tend to have some associated promiscuity),[18,19] an increase in solubility (better permeability and exposure), and better occupancy of the binding pocket (which may provide better target specificity). A suitable value is reported to be $F_{sp^3} \geq 0.42$; however, compound **3** falls below this value ($F_{sp^3} = 0.27$).[20] Thus, our optimization efforts focused on improving the lipophilic efficiency to mitigate metabolic liabilities while retaining potency and HMT selectivity.

During analogue design, compounds biased to reside in the cis conformation were prioritized because the cocrystal structure of **3** suggested that this would best mimic the planar aromatic ring seen in the early leads **2** and **3** (Figure 1).[14] Subsequent conformational analysis showed that *cis*-cyclohexanes would have a strong energetic bias to reside in conformer **I**, thereby avoiding 1,3-diaxial strain from the 1,3-disubstitution (Figure 2), and this was supported by molecular dynamics simulations. Molecular modeling predicted conformer **I** to bind well in the ligand pocket compared with the *trans*-cyclohexane in conformers **III** and **IV**, where the conformational changes of the

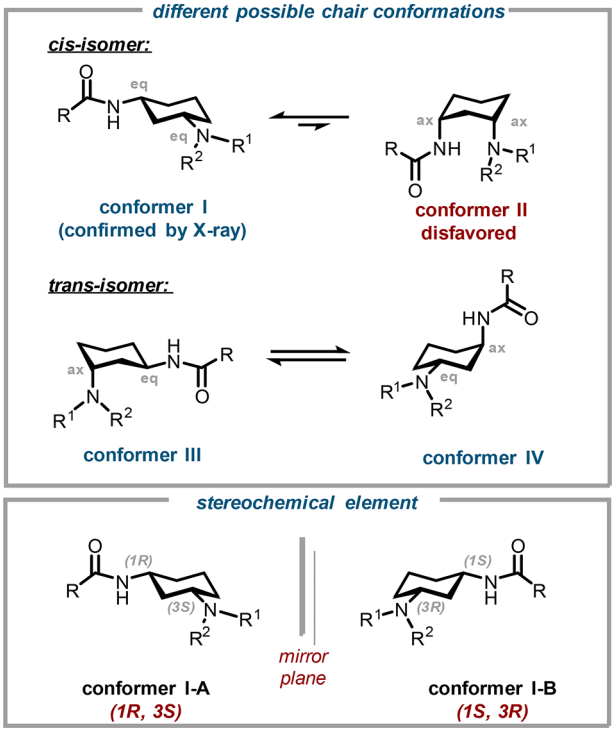

Figure 2. Potential chair conformational isomers of *cis*- and *trans*-(1,3)-diaminocyclohexyl analogues and stereochemical considerations.

https://doi.org/10.1021/acsmedchemlett.2c00167
ACS Med. Chem. Lett. 2022, 13, 1137−1143

Scheme 1. Synthesis of Stereoisomers of EZM0414 and Synthetic Strategy for Advanced Analogues 7-9

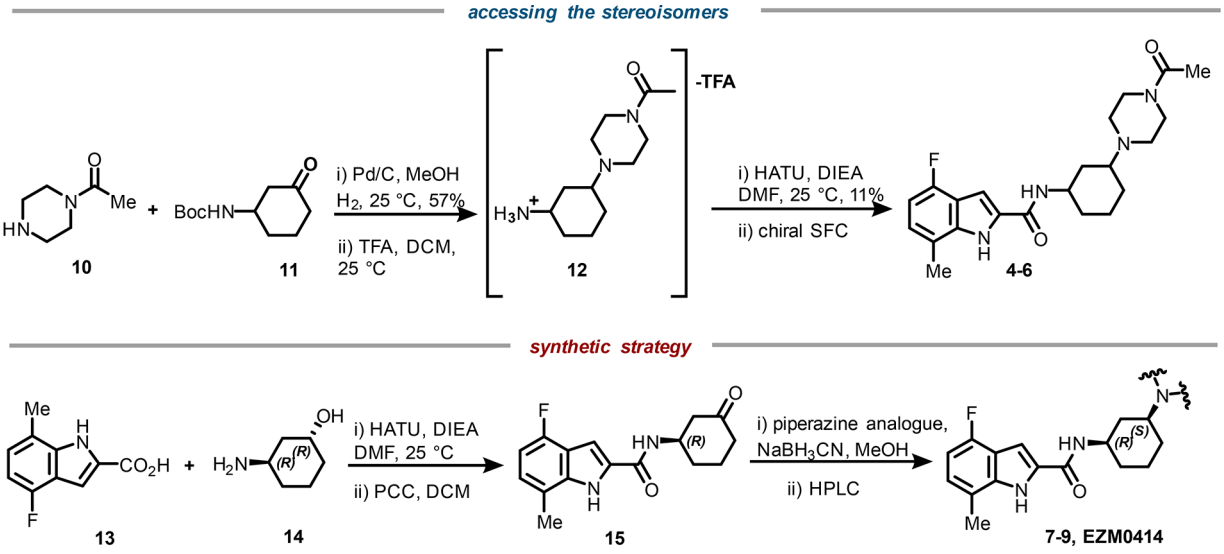

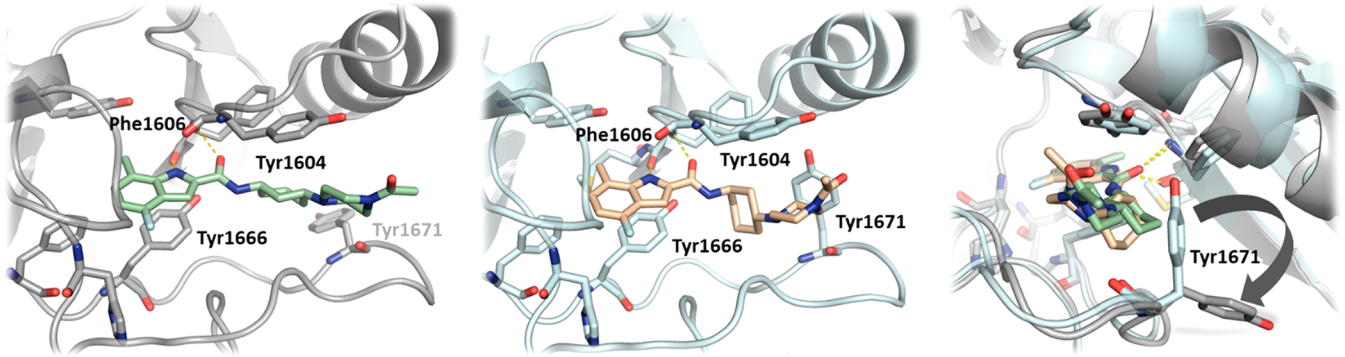

Figure 3. (left) X-ray cocrystal structure of SETD2 and EZM0414 (in pale green) (PDB ID 7TY2), (middle) X-ray cocrystal structure of SETD2 and **6** (in wheat) (PDB ID 7TY3), and (right) overlay showing Tyr1671 movement (90° rotation). SAM is present in both structures but has been omitted for clarity in the renderings. See the Supporting Information for details.

ligand binding site would be less tolerated because of the axial substituent (see the Supporting Information). Analysis of the chair structures for conformer **I** in the binding site with replacement of compound **2** in the cocrystal structure shown in Figure 1 suggested that there could be a stereochemical preference within the *cis*-cyclohexane conformations (**I-A** and **I-B**). To better understand this, both *cis*- and *trans*-(1,3)-diaminocyclohexanes were initially prepared simultaneously from racemic starting materials and isolated *via* chiral resolution of the diastereomeric product mixture, as shown in Scheme 1 (top). The relative stereochemistry of each stereocenter in **4**−**6** was determined *via* 2D NMR experiments after chiral separation. The collection of biochemical data for each (1*S*/*R*,3*S*/*R*) stereoisomer revealed that there was indeed a preferred *cis*-chair conformation along with a stereochemical preference for the 1*R* configuration at the carboxamide junction resulting in greater activity. The absolute stereochemistry of the most active isomer, EZM0414, was confirmed to be (1*R*,3*S*) *via* X-ray crystallography, which was consistent with the stereochemistry of the starting (1*R*,3*R*)-3-aminocyclohexan-1-ol **14** upon resynthesis, as shown in Scheme 1 (bottom). This alternative route utilizing chiral starting materials was also employed with an emphasis on piperazine analogues and the corresponding bioisosteres (Scheme 1, bottom).

The conformational impact of the cyclohexyl region was confirmed with a cocrystal of EZM0414 and its diastereomer **6** bound to SETD2, as rendered in Figure 3. In both structures, the indole motif is positioned deep within the lysine channel with two specific hydrogen bonds to the main-chain atoms of Phe1606, consistent with our earlier series exemplified by **3**. In the bound conformation, a well-ordered water network suggests the possibility of a water-mediated hydrogen-bonding interaction between the carboxamide and the nearest acceptor residue, Gln1676. With EZM0414, the cyclohexyl ring adopts a rigid *cis*-chair conformation stabilizing the Tyr1671 residue in an "out" position *via* a hydrophobic interaction. The (1*R*,3*S*) stereochemistry of the ring serves to orient the piperazine substituent in an appropriate direction toward the solvent. With **6**, the cyclohexyl ring adopts a *trans*-chair conformation that allows the Tyr1671 residue to be in an "in" position, and the (1*R*,3*S*) stereochemistry of the ring gives preference to the piperazine for the equatorial position (conformer IV in Figure 2).

Since oxidation of tertiary amines is a common metabolic pathway, we postulated that cyclization at the α-position of the piperazine or the *N*-acetamide might mitigate this risk and potentially lead to further improvements in the overall PK properties. Some of the most potent examples (**7**−**9**) are shown

https://doi.org/10.1021/acsmedchemlett.2c00167
ACS Med. Chem. Lett. 2022, 13, 1137−1143

Chart 1. Stereoisomers Leading to EZM0414 and Advanced Analogues

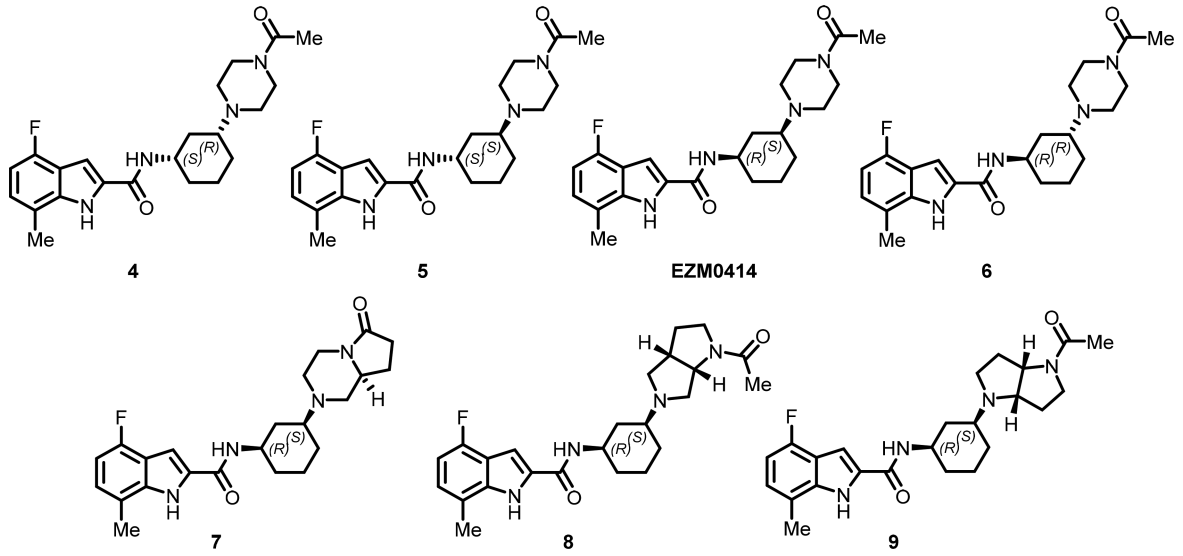

Table 1. Conformational Activities and Profiles of Advanced Analogues

compound	diaminocyclohexyl stereochemistry[b]	SETD2 activity IC_{50} (μM)[a] biochemical[c]	SETD2 activity IC_{50} (μM)[a] H3K36me3 ICW[d]	14-day antiproliferation EC_{50} (μM)[a,e]	cLogP
EPZ-719	(1*R*,3*S*)	0.008 ± 0.003	0.020 ± 0.008	0.025 ± 0.003	1.46
3	achiral	0.027 ± 0.006	0.134 ± 0.066	0.245	2.92
3-F	achiral	0.012 ± 0.017	0.041 ± 0.002	0.060	3.07
4	(1*S*,3*R*)	>10	>2	>10	1.85
5	(1*S*,3*S*)	>10	>2	>10	1.85
EZM0414	(1*R*,3*S*)	0.018 ± 0.009	0.031 ± 0.014	0.057 ± 0.003	1.85
6	(1*R*,3*R*)	1.24 ± 0.66	>2	7.79	1.85
7	(1*R*,3*S*)	0.015 ± 0.009	0.011 ± 0.003	0.015	2.13
8	(1*R*,3*S*)	0.011 ± 0.003	0.014 ± 0.002	0.027	1.97
9	(1*R*,3*S*)	0.009 ± 0.002	0.005 ± 0.001	0.017	1.91

[a]Data are reported as geometric means of at least two test results. [b]Absolute stereochemistries were determined by 2D NMR spectroscopy and X-ray crystallography. [c]SETD2 biochemical assay. [d]Cellular potency in the A549 cell line. [e]KMS-34 cells were incubated with compound for 14 days.

in Chart 1, including [5,5]-fused and [5,6]-fused cyclic analogues. Ultimately, these advanced analogues **7**–**9** exhibited excellent potency in both our molecular and cellular assays. These compounds were synthesized as mixtures of diastereomers from chiral intermediate **15**, starting from **14** following a previously reported reaction sequence. The HATU-mediated coupling of **13** and **14** followed by oxidation of the intermediate alcohol gave ketone **15**. The piperazine analogues could be installed *via* reductive amination and subsequent chiral resolution, and the most potent diastereomer is reported in Table 1. While absolute stereochemistry was not routinely determined, 2D NMR techniques were employed to assign relative cis/trans stereochemistry for the final compounds (see the Supporting Information).

With the improved cyclohexyl series, it became evident that we were approaching the enzymatic assay limits and could no longer reliably rank-order the compound potencies on the basis of this parameter alone. We sought to probe the response to SETD2 inhibition in a subset of cell lines that would be sensitive to SETD2 inhibition, mainly featuring a t(4,14) translocation. As can be seen in Table 1, we assessed the growth inhibition in KMS-34 cells after 14 days of compound treatment. With this series, cellular potency translated well to our long-term proliferation (LTP) assays, with potent growth inhibition observed with EZM0414 and compounds **7**–**9**.

We next sought to identify a drug candidate with optimized PK and safety profiles to support once-daily dosing in the clinic. Further ADME profiling of EZM0414 and analogues **7**–**9** (Table 2) showed an improvement in hepatocyte stability compared with **3**. Further characterization of piperazine bioisosteres **8** and **9** revealed that they suffered from poor

Table 2. *In Vitro* ADME for Advanced Analogues

compound	permeability: Caco-2 P_{app} (a-b:b-a) (10^{-6} cm/s)[a]	stability in hepatocytes: scaled h/r/m Cl_{int} (mL min^{-1} kg^{-1})[b]
EPZ-719	3.2:18	51/137/721
3	6.3:5.2	32/283/678
EZM0414	3.2:20	9/154/216
7	4.3:17	23/69/425
8	<1.0:32	18/265/889
9	<1.0:22	5/72/103

[a]Parent compound (5 μM) was incubated for 2 h at 37 °C. [b]Parent compound (0.5 μM) was incubated for 60 min for mouse (m) and rat (r) hepatocytes and 120 min for human (h) hepatocytes. See the Supporting Information for details.

https://doi.org/10.1021/acsmedchemlett.2c00167
ACS Med. Chem. Lett. 2022, 13, 1137−1143

apparent permeability *in vitro*. Despite subsequent mouse PK studies showing compounds **8** and **9** to have reasonable oral absorption, 17−30% of the parent was recovered in feces following iv administration, suggesting moderate direct elimination as a clearance mechanism (data not shown). While both EZM0414 and analogue **7** showed favorable PK profiles following 50 mg/kg po administration in mice, EZM0414 had ∼2-fold higher exposure (AUC) with better oral bioavailability (F) than **7**, a trend that was observed in rats as well. Table 3 presents a comparison of the PK parameters for

Table 3. Comparison of Pharmacokinetic Parameters of 3, EZM0414, and 7 Following Intravenous and Oral Administration

parameter	3	EZM0414	7
CD-1 IGS Mouse[a]			
dose (mg/kg) iv/po	2/50	2/50	1/50
Cl (mL min^{-1} kg^{-1})[b] iv	36	43	35
V_{ss} (L/kg)[c] iv	1.1	4.7	2.9
C_{max} (μg/mL)[d] po	0.5	8.6	7.6
AUC (μg h/mL)[e] iv/po	0.9/1.6	0.8/27	0.5/14
$t_{1/2}$ (h)[f] iv/po	0.4/0.8	1.8/1.8	1.6/0.8
F (%)[g] po	7	>100	55
Sprague−Dawley Rat[a]			
dose (mg/kg) iv/po	2/10	2/10	1/10
Cl (mL min^{-1} kg^{-1})[b] iv	19	16.2	14
V_{ss} (L/kg)[c] iv	0.65	4.1	2.7
C_{max} (μg/mL)[d] po	0.2	2.1	1.6
AUC (μg h/mL)[e] iv/po	2.3/0.7	2.1/10.5	1.3/7.7
$t_{1/2}$ (h)[f] iv/po	0.8/2.3	4.0/3.8	4.1/2.7
F (%)[g] po	6.2	97	60

[a]Data are reported as averages over at least two animals. [b]*In vivo* clearance. [c]Volume of distribution at steady state. [d]Maximum concentration. [e]Area under the concentration−time curve from zero to infinity. [f]Elimination half-life. [g]Oral bioavailability. Oral dosing solutions were prepared using 0.5% CMC and 0.1% Tween in water at pH 4.

EZM0414, **7**, and the starting parent compound **3**. Improving the lipophilic efficiency of the earlier series vastly enhanced the overall PK profile, with a 17-fold increase in overall exposure levels ($AUC_{0-\infty}$) achieved in CD-1 mice at 50 mg/kg following oral administration with EZM0414. With regard to the potential for drug−drug interactions as perpetrator of CYP enzymes, EZM0414 exhibited only weak inhibition of CYP isoform 2C8 (4.8 μM), and no inhibition of other tested isoforms was seen (IC_{50} > 30 μM for isoforms 1A2, 2B6, 2C9, 2C19, 2D6, and 3A4). Analogue **7** showed modest inhibition of isoforms 2B6 (3.2 μM) and 2D6 (10.8 μM), with IC_{50} > 25 μM for the remaining isoforms tested. Additional characterization of EZM0414 indicated a favorable safety pharmacology profile. *In vitro* testing of EZM0414 in a safety panel consisting of 47 targets and a diversity panel of 72 kinases showed IC_{50} > 25 μM for all targets except D_2 (IC_{50} = 13.0 μM, antagonist) and 5-HT_{1B} (IC_{50} = 3.2 μM, agonist).

To demonstrate the impact of SETD2 inhibition on H3K36me3 levels and tumor growth *in vivo*, we conducted an *in vivo* efficacy study with EZM0414 in a NOD SCID mouse xenograft model implanted with human KMS-11 cells (multiple myeloma cell line; 14-day LTP IC_{50} = 370 ± 224 nM). Daily dosing of 15 and 30 mg/kg EZM0414 bid in mice was well-tolerated and induced tumor growth reductions of 60 and 91%, respectively (Figure 4). EZM0414 exhibited dose-proportional exposures at both doses tested (Table 4). Further analysis of

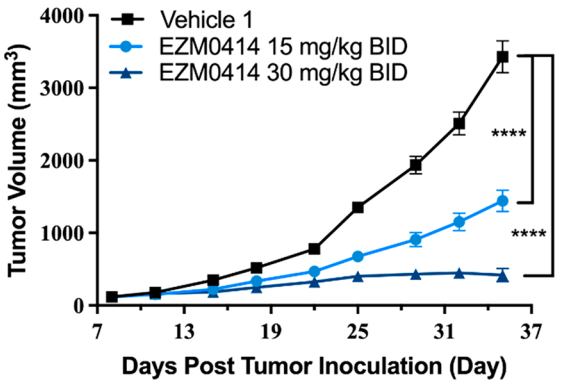

Figure 4. *In vivo* efficacy with EZM0414, dosed twice daily in a KMS-11 cell line-derived xenograft model. ****, p < 0.00001.

Table 4. PK−PD Relationship of EZM0414 in a KMS-11 Xenograft Tumor Mouse Model

PO dose (mg/kg)[a]	AUC (μg h/mL)[b]	PD (%)[c]
15	9.4	90
30	21.4	93

[a]bid po dosing, prepared using 0.5% CMC and 0.1% Tween in water at pH 4. [b]Area under the plasma concentration−time curve from zero to 24 h after last dose. [c]Percent reduction in H3K36me3 measured in the tumor 12 h after last dose compared with vehicle.

intratumoral H3K36me3 levels taken from samples 12 h after administration of the last dose showed a significant modulation of H3K36me3 expression, demonstrating on-target inhibition of SETD2 methyltransferase activity *in vivo*.

In summary, structure-based drug design and conformational analysis of 1,3-disubstituted cyclohexanes were considered in designing a replacement for the aromatic core found in compounds **2** and **3**. Evaluation of the different possible cyclohexyl isomers identified an active cis stereoisomer, and the absolute stereochemistry was confirmed to be (1*R*,3*S*). The strategic increase in F_{sp^3} resulted in a decrease in lipophilicity and led to the identification of EZM0414, a potent and selective inhibitor of SETD2 with good pharmacokinetic properties. For these reasons, EZM0414 was progressed through IND-enabling studies and is undergoing Phase 1 clinical trials.

■ ASSOCIATED CONTENT

Supporting Information

The Supporting Information is available free of charge at https://pubs.acs.org/doi/10.1021/acsmedchemlett.2c00167.

Synthetic procedures for all compounds; biochemical, cellular, ADME, and pharmacokinetic assay protocols; and crystallography protocols (PDF)

■ AUTHOR INFORMATION

Corresponding Author

Neil A. Farrow − *Epizyme Inc., Cambridge, Massachusetts 02139, United States;* orcid.org/0000-0002-1469-0466; Email: nfarrow@epizyme.com

https://doi.org/10.1021/acsmedchemlett.2c00167
ACS Med. Chem. Lett. 2022, 13, 1137−1143

Authors

Joshua S. Alford − *Epizyme Inc., Cambridge, Massachusetts 02139, United States*

John W. Lampe − *Epizyme Inc., Cambridge, Massachusetts 02139, United States*

Dorothy Brach − *Epizyme Inc., Cambridge, Massachusetts 02139, United States*

Richard Chesworth − *Epizyme Inc., Cambridge, Massachusetts 02139, United States*

Kat Cosmopoulos − *Epizyme Inc., Cambridge, Massachusetts 02139, United States*

Kenneth W. Duncan − *Epizyme Inc., Cambridge, Massachusetts 02139, United States;* Present Address: Accent Therapeutics, 65 Hayden Avenue, Lexington, MA 02421, United States

Sean T. Eckley − *Epizyme Inc., Cambridge, Massachusetts 02139, United States*

Jeffrey L. Kutok − *Epizyme Inc., Cambridge, Massachusetts 02139, United States*

Alejandra Raimondi − *Epizyme Inc., Cambridge, Massachusetts 02139, United States*

Thomas V. Riera − *Epizyme Inc., Cambridge, Massachusetts 02139, United States*

Brian Shook − *Epizyme Inc., Cambridge, Massachusetts 02139, United States*

Cuyue Tang − *Epizyme Inc., Cambridge, Massachusetts 02139, United States;* Present Address: Remix Therapeutics, One Kendall Square, Building 200, Cambridge, MA 02139, United States

Jennifer Totman − *Epizyme Inc., Cambridge, Massachusetts 02139, United States*

Complete contact information is available at: https://pubs.acs.org/10.1021/acsmedchemlett.2c00167

Author Contributions

The manuscript was written through contributions of all authors.

Funding

This work was funded by Epizyme, Inc.

Notes

All of the procedures related to animal handling, care, and treatment in this study were performed according to the guidelines approved by the Institutional Animal Care and Use Committee of Pharmaron (Beijing, China) and following the guidance of the Association for Assessment and Accreditation of Laboratory Animal Care.

The authors declare the following competing financial interest(s): All of the authors are/were employees of Epizyme, Inc.

The coordinates of SETD2 in complex with EZM0414 and **6** have been deposited in the Protein Data Bank under PDB IDs 7TY2 and 7TY3, respectively.

■ ACKNOWLEDGMENTS

The authors gratefully acknowledge the efforts of current and former Epizyme colleagues who contributed to various aspects of the SETD2 research program.

■ ABBREVIATIONS

tPSA, total polar surface area; PK, pharmacokinetics; ADME, absorption, distribution, metabolism, and excretion; iv, intravenous; po, oral dosing; MeOH, methanol; HATU, 1-[bis(dimethylamino)methylene]-1*H*-1,2,3-triazolo[4,5-*b*]pyridinium-3-oxide hexafluorophosphate; bid, twice per day dosing

■ REFERENCES

(1) Yu, C.; Zhuang, S. Histone Methyltransferases as Therapeutic Targets for Kidney Diseases. *Front. Pharmacol* **2019**, *10*, 1393.

(2) Li, J.; Duns, G.; Westers, H.; Sijmons, R.; van den Berg, A.; Kok, K. SETD2: an epigenetic modifier with tumor suppressor functionality. *Oncotarget* **2016**, *7* (31), 50719−50734.

(3) Hart, T.; Chandrashekhar, M.; Aregger, M.; Steinhart, Z.; Brown, K. R.; MacLeod, G.; Mis, M.; Zimmermann, M.; Fradet-Turcotte, A.; Sun, S.; Mero, P.; Dirks, P.; Sidhu, S.; Roth, F. P.; Rissland, O. S.; Durocher, D.; Angers, S.; Moffat, J. High-Resolution CRISPR Screens Reveal Fitness Genes and Genotype-Specific Cancer Liabilities. *Cell* **2015**, *163* (6), 1515−26.

(4) Mar, B. G.; Chu, S. H.; Kahn, J. D.; Krivtsov, A. V.; Koche, R.; Castellano, C. A.; Kotlier, J. L.; Zon, R. L.; McConkey, M. E.; Chabon, J.; Chappell, R.; Grauman, P. V.; Hsieh, J. J.; Armstrong, S. A.; Ebert, B. L. SETD2 alterations impair DNA damage recognition and lead to resistance to chemotherapy in leukemia. *Blood* **2017**, *130* (24), 2631−2641.

(5) Reddy, A.; Zhang, J.; Davis, N. S.; Moffitt, A. B.; Love, C. L.; Waldrop, A.; Leppa, S.; Pasanen, A.; Meriranta, L.; Karjalainen-Lindsberg, M. L.; Norgaard, P.; Pedersen, M.; Gang, A. O.; Hogdall, E.; Heavican, T. B.; Lone, W.; Iqbal, J.; Qin, Q.; Li, G.; Kim, S. Y.; Healy, J.; Richards, K. L.; Fedoriw, Y.; Bernal-Mizrachi, L.; Koff, J. L.; Staton, A. D.; Flowers, C. R.; Paltiel, O.; Goldschmidt, N.; Calaminici, M.; Clear, A.; Gribben, J.; Nguyen, E.; Czader, M. B.; Ondrejka, S. L.; Collie, A.; Hsi, E. D.; Tse, E.; Au-Yeung, R. K. H.; Kwong, Y. L.; Srivastava, G.; Choi, W. W. L.; Evens, A. M.; Pilichowska, M.; Sengar, M.; Reddy, N.; Li, S.; Chadburn, A.; Gordon, L. I.; Jaffe, E. S.; Levy, S.; Rempel, R.; Tzeng, T.; Happ, L. E.; Dave, T.; Rajagopalan, D.; Datta, J.; Dunson, D. B.; Dave, S. S. Genetic and Functional Drivers of Diffuse Large B Cell Lymphoma. *Cell* **2017**, *171* (2), 481−494.

(6) Shi, J.; Wang, E.; Milazzo, J. P.; Wang, Z.; Kinney, J. B.; Vakoc, C. R. Discovery of cancer drug targets by CRISPR-Cas9 screening of protein domains. *Nat. Biotechnol.* **2015**, *33* (6), 661−7.

(7) Skucha, A.; Ebner, J.; Grebien, F. Roles of SETD2 in Leukemia—Transcription, DNA-Damage, and Beyond. *Int. J. Mol. Sci.* **2019**, *20* (5), No. 1029.

(8) Tzelepis, K.; Koike-Yusa, H.; De Braekeleer, E.; Li, Y.; Metzakopian, E.; Dovey, O. M.; Mupo, A.; Grinkevich, V.; Li, M.; Mazan, M.; Gozdecka, M.; Ohnishi, S.; Cooper, J.; Patel, M.; McKerrell, T.; Chen, B.; Domingues, A. F.; Gallipoli, P.; Teichmann, S.; Ponstingl, H.; McDermott, U.; Saez-Rodriguez, J.; Huntly, B. J. P.; Iorio, F.; Pina, C.; Vassiliou, G. S.; Yusa, K. A CRISPR Dropout Screen Identifies Genetic Vulnerabilities and Therapeutic Targets in Acute Myeloid Leukemia. *Cell Rep.* **2016**, *17* (4), 1193−1205.

(9) Wang, T.; Birsoy, K.; Hughes, N. W.; Krupczak, K. M.; Post, Y.; Wei, J. J.; Lander, E. S.; Sabatini, D. M. Identification and characterization of essential genes in the human genome. *Science* **2015**, *350* (6264), 1096−101.

(10) Kuo, A. J.; Cheung, P.; Chen, K.; Zee, B. M.; Kioi, M.; Lauring, J.; Xi, Y.; Park, B. H.; Shi, X.; Garcia, B. A.; Li, W.; Gozani, O. NSD2 links dimethylation of histone H3 at lysine 36 to oncogenic programming. *Mol. Cell* **2011**, *44* (4), 609−20.

(11) Yusufova, N.; Kloetgen, A.; Teater, M.; Osunsade, A.; Camarillo, J. M.; Chin, C. R.; Doane, A. S.; Venters, B. J.; Portillo-Ledesma, S.; Conway, J.; Phillip, J. M.; Elemento, O.; Scott, D. W.; Beguelin, W.; Licht, J. D.; Kelleher, N. L.; Staudt, L. M.; Skoultchi, A. I.; Keogh, M. C.; Apostolou, E.; Mason, C. E.; Imielinski, M.; Schlick, T.; David, Y.; Tsirigos, A.; Allis, C. D.; Soshnev, A. A.; Cesarman, E.; Melnick, A. M. Histone H1 loss drives lymphoma by disrupting 3D chromatin architecture. *Nature* **2021**, *589* (7841), 299−305.

(12) Edmunds, J. W.; Mahadevan, L. C.; Clayton, A. L. Dynamic histone H3 methylation during gene induction: HYPB/Setd2 mediates all H3K36 trimethylation. *EMBO J.* **2008**, *27* (2), 406−20.

(13) Sun, X. J.; Wei, J.; Wu, X. Y.; Hu, M.; Wang, L.; Wang, H. H.; Zhang, Q. H.; Chen, S. J.; Huang, Q. H.; Chen, Z. Identification and characterization of a novel human histone H3 lysine 36-specific methyltransferase. *J. Biol. Chem.* **2005**, *280* (42), 35261−71.
(14) Lampe, J. W.; Alford, J. S.; Boriak-Sjodin, P. A.; Brach, D.; Cosmopoulos, K.; Duncan, K. W.; Eckley, S. T.; Foley, M. A.; Harvey, D. M.; Motwani, V.; Munchhof, M. J.; Raimondi, A.; Riera, T. V.; Tang, C.; Thomenius, M. J.; Totman, J.; Farrow, N. A. Discovery of a First-in-Class Inhibitor of the Histone Methyltransferase SETD2 Suitable for Preclinical Studies. *ACS Med. Chem. Lett.* **2021**, *12* (10), 1539−1545.
(15) Sodano, T. M.; Combee, L. A.; Stephenson, C. R. J. Recent Advances and Outlook for the Isosteric Replacement of Anilines. *ACS Med. Chem. Lett.* **2020**, *11* (10), 1785−1788.
(16) *A Study in Subjects with Relapsed/Refractory Multiple Myeloma and Relapsed/Refractory Diffuse Large B-Cell Lymphoma*. Clinical Trial NCT05121103. https://clinicaltrials.gov/ct2/show/NCT05121103.
(17) Wei, W.; Cherukupalli, S.; Jing, L.; Liu, X.; Zhan, P. Fsp(3): A new parameter for drug-likeness. *Drug Discovery Today* **2020**, *25* (10), 1839−1845.
(18) Peters, J. U.; Schnider, P.; Mattei, P.; Kansy, M. Pharmacological promiscuity: dependence on compound properties and target specificity in a set of recent Roche compounds. *ChemMedChem* **2009**, *4* (4), 680−6.
(19) Yukawa, T.; Naven, R. Utility of Physicochemical Properties for the Prediction of Toxicological Outcomes: Takeda Perspective. *ACS Med. Chem. Lett.* **2020**, *11* (2), 203−209.
(20) Kombo, D. C.; Tallapragada, K.; Jain, R.; Chewning, J.; Mazurov, A. A.; Speake, J. D.; Hauser, T. A.; Toler, S. 3D molecular descriptors important for clinical success. *J. Chem. Inf. Model.* **2013**, *53* (2), 327−42.

https://doi.org/10.1021/acsmedchemlett.2c00167
ACS Med. Chem. Lett. 2022, 13, 1137−1143